Direct evaluation of S-wave amplification factors from microtremor H/V ratios: Double empirical corrections to “Nakamura” method

Kawase, Hiroshi; Nagashima, Fumiaki; Nakano, Kenichi; Mori, Yuta

CITATION:

Kawase, Hiroshi ...[et al]. Direct evaluation of S-wave amplification factors from microtremor H/V ratios: Double empirical corrections to “Nakamura” method. Soil Dynamics and Earthquake Engineering 2019, 126: 105067.

ISSUE DATE:

2019-11

URL:

http://hdl.handle.net/2433/254108

Soil Dynamics and Earthquake Engineering 126 (2019) 105067

Contents lists available at ScienceDirect

Soil Dynamics and Earthquake Engineering

journal homepage: www.elsevier.com/locate/soildyn

Direct evaluation of S-wave amplification factors from microtremor H/V ratios: Double empirical corrections to "Nakamura" method

Hiroshi Kawase[a,*], Fumiaki Nagashima[a], Kenichi Nakano[b], Yuta Mori[c]

[a] DPRI, Kyoto University, Gokasho, Uji, Japan
[b] HAZAMA-ANDO Corp., Tsukuba, Japan
[c] J-Power, Chuo-ku, Tokyo, Japan

ARTICLE INFO

Keywords:
H/V ratios
Ground motions
Microtremors
Generalized inversion
S-wave
Site amplification factor

ABSTRACT

The Horizontal-to-Vertical spectral ratios of microtremors (MHVR) have been utilized as a convenient tool to extract a predominant frequency at a target site. The so-called "Nakamura" method, which was proposed by Nakamura in 80's, assumed that MHVR provides us directly the S-wave amplification factor of earthquake in the horizontal component, that is, Horizontal-to-Horizontal spectral ratio (HHR) with respect to the bedrock, although the validity of the method had never been proved. Recently, based on the diffuse field concept (DFC) proposed by Sánchez-Sesma and others in 2011 MHVRs are found to correspond to the square root of the ratio of the imaginary part of the displacement for a unit harmonic load in the horizontal direction with respect to the corresponding one in the vertical direction. With the same DFC for body waves Horizontal-to-Vertical spectral ratios of earthquake (EHVR) correspond to the ratio of the horizontal motion for a vertical incidence of S wave with respect to the vertical correspondent of P wave, as revealed by Kawase and others in 2011. Thus there should be a systematic difference between EHVR and MHVR because of the difference in their primary contribution of wave types. We first calculated the ratios of EHVR with respect to MHVR (EMR) at 100 strong motion stations in Japan. Then we normalized frequency by the fundamental peak frequency at each site and calculated the average of EMRs for five categories based on their fundamental peak frequencies. Once we got empirical EMRs for five categories we transformed MHVRs into pseudo EHVRs. At the same time we calculated the average Vertical-to-Vertical spectral ratios (VVRs) for the same sites using the generalized spectral inversion technique (GIT) of Nakano et al. (2015) [16]. Finally the S-wave amplification factor, HHR, of earthquake ground motion at the site were calculated from MHVR with double corrections using EMR and VVR for the corresponding category. We compared these final empirical prediction with the observed HHRs from GIT to find quite high correlations and small overall residuals. The proposed method to get HHR from MHVR with these double empirical corrections can be considered as a natural but significant extension to the so-called "Nakamura" method.

1. Introduction

It is essential for quantitative evaluation of seismic hazard to evaluate the site amplification factors as precisely as possible since the effects of site amplification are quite significant, especially for sites on the thick, soft sediments where most of the contemporary urban environments have been built.

One approach to this end is to delineate and validate either a local or regional subsurface structure based on the available geological data, boring explorations, and/or other non-invasive seismic and non-seismic

Abbreviations: DFC, Diffuse Field Concept; EHVR, Earthquake Horizontal-to-Vertical spectral Ratio; EMR, Earthquake-to-Microtremor Ratio in the horizontal-to-vertical spectral ratio; EW, East-West; FAS, Fourier Amplitude Spectra; f_{peak}, fundamental peak frequency in MHVR; GIT, Generalized spectral Inversion Technique; GMPE, Ground Motion Prediction Equation; HHR, Horizontal-to-Horizontal spectral Ratio, a short form of HH_bR; HH_bR, Horizontal-to-Horizontal bedrock motion spectral Ratio; HVR, Horizontal-to-Vertical spectral Ratio; JMA, Japan Meteorological Agency; K-NET, Kyoshin Network; KiK-net, Kiban Kyoshin network; MHVR, Microtremor Horizontal-to-Vertical spectral Ratio; MVHR, Microtremor Vertical-to-Horizontal spectral Ratio; NIED, National Institute for Earth Science and Disaster Resilience; NS, North-South; pEHVR, pseudo EHVR, reproduced from EMR and MHVR; pHH_bR, pseudo HH_bR, reproduced HH_bR from double empirical correction; pVH_bR, pseudo VH_bR, averaged VH_bRs for five categories; PGA, Peak Ground Acceleration; PGV, Peak Ground Velocity; RMS, Root-Mean-Square; RS, Response Spectra; UD, Up-Down; VH_bR, Vertical-to-Horizontal bedrock motion spectral Ratio; V_bH_bR, Vertical bedrock motion-to-Horizontal bedrock motion spectral Ratio; VVR, Vertical-to-Vertical spectral Ratio, a short form of VV_bR; VV_bR, Vertical-to-Vertical bedrock motion spectral Ratio

* Corresponding author.
E-mail addresses: kawase@zeisei.dpri.kyoto-u.ac.jp (H. Kawase), nagashima@zeisei.dpri.kyoto-u.ac.jp (F. Nagashima), nakano.kenichi@ad-hzm.co.jp (K. Nakano), yuta_mori@jpower.co.jp (Y. Mori).

https://doi.org/10.1016/j.soildyn.2018.01.049
Received 28 July 2017; Received in revised form 19 December 2017; Accepted 31 January 2018
Available online 23 February 2018

techniques of underground explorations and then use numerical simulation methods to predict strong motions amplification factors at a target site. There are plenty of methods to evaluate subsurface structures that may use to reproduce site characteristics of observed ground motions. However, there are not so many methods that can reliably determine S-wave velocity structures down to the seismological bedrock, where the S-wave velocity reach 3.0 km/s or higher. Many studies show that it is important to evaluate site amplification factors from the seismological bedrock, not from the engineering bedrock (a firm layer below soft sediments) or hard rock outcrop, since that is the only layer where waves from the source are impinging without having any site amplification.

Array measurements of microtremors to obtain phase velocities of propagating surface waves (e.g., [1,2]) have been successfully utilized to invert S-wave velocity structures down to the seismological bedrock for more than three decades. Recent advances [3] and [4] as a natural extension of the pioneering work of the so-called SPAC method proposed originally by Aki [5] provide us quite a strong tool for dispersion analysis of propagating surface waves. The downside of these array methods is that we need to deploy as many stations as possible for precise determination of phase velocity at one frequency band and the array size must be increased in proportion to the targeted depth or phase velocity. As the array size is increased, the fundamental assumption of horizontally homogeneous layering would be difficult to expect. Also these array methods require very low-noise sensors with high coherence, especially in the long period range. On the other hand boring measurements down to the seismological bedrock are prohibitively expensive as is the case for wide-range reflection survey for a deep-basin site.

The other approach to evaluate the site amplification factors is to utilize directly the observed data. To refer to both site-specific (i.e., single site) description as well as categorized average value prediction we refer to such a method as the empirical approach in contrast to the aforementioned theoretical approach. The simplest empirical approach is the one used in most of the ground motion prediction equations (GMPEs) for selected strength index of ground motion, such as a peak ground acceleration (PGA), a peak ground velocity (PGV), or response spectra at prescribed oscillatory frequencies of a pendulum (RS), for which we have relative site factors as values depending on the predefined site category or information. The most frequently used single parameter for such an empirical site factor is Vs30, the average S-wave velocity for top 30 m at the site as shown in the recent literature on GMPEs [6–9].

The drawback of these empirical approaches for ground motion strength indices lies in that it is difficult to interpret physically the calculated value, since these strength indices are the resultant entity as a mixture of different contributions in terms of space and frequency (see for example Bora et al., for RS [10]). Theoretically Fourier amplitude spectra (FAS) is much easier to attribute observed characteristics to physical parameters from a source to a site because of the perfect orthogonality between different frequencies.

The spectral ratio approach for FAS with a reference site for seismic motions, either on the surface or inside the borehole, can be quite effective to obtain a real site amplification factors [11,12], from which we can invert a reliable S-wave velocity structure when combined with a standard inversion technique such as Genetic Algorithm for a one-dimensional (1-D) stack of layers. However, such a simple spectral-ratio approach with respect to the rock outcrop reference site, sometimes called standard spectral ratio method [e.g., 13], will fail to provide reasonable site amplification factors either when the reference site is not sufficiently close to the target site, or when the reference site is not close to the seismological bedrock in terms of its S-wave velocity. On the other hand the so-called generalized spectral inversion technique (GIT) will provide better site amplification factors if we find a good reference site among stations used [14], because the generalized inversion makes use of all the data at once with proper attenuation correction and so the distance between the reference site and the target site will be no longer the issue. In the recent work using GIT for K-NET, KiK-net, and the JMA Shindokei network data in Japan [15,16] the site amplification factors relative to the seismological bedrock outcrop at the reference site (YMGH01) were obtained and then used to invert S-wave velocity structures at these sites. The resultant velocity structures at KiK-net sites are found to be similar to the downhole S-wave loggings in general, although they almost never exactly match each other.

As for the borehole-to-surface spectral ratio method there is no difficult issue associated with the distance since the location of two sensors should be close together in a horizontal space. However, it is also quite a common situation to have a reference site not close to the seismological bedrock depth, especially for deep sedimentary basin sites, either due to the cost of boring or high temperature in the borehole. Even if the borehole station were well within a seismological bedrock formation, the borehole-to-surface spectral ratio is contaminated by the reflected phase at the free surface [17,18] or [11,12]. Besides it is quite costly to deploy two sensors at the top and the bottom of the borehole, which should be sufficiently deep to reach the seismological bedrock.

Recently using the cross-correlation of observed ground motions at two stations the so-called Green's function retrieval method based on the diffuse field concept (DFC) has been proposed and commonly applied to both seismic data and long-duration of microtremor data [e.g., 19]. This is quite a powerful tool to use as a substitute of the Green's function between two stations directly [e.g., 20] or to determine a velocity structure averaged over the whole path between two stations based on the dispersion characteristics of the obtained Green's functions [e.g., 21]. However, it does not provide amplification factors immediately below the observed site. Besides it may need to measure microtremors for sufficiently long duration (from several weeks to months) to get stable results.

After successful application of the cross-correlation analysis of earthquake and microtremor data, it is natural to make two stations coincide to each other, that is, to utilize the auto-correlation of a single station measurement. In the auto-correlation approach we can determine the velocity structure immediately below the observed site because of the direct correspondence of the imaginary part of the Green's function to the spectral energy density (Sánchez-Sesma, et al., 2011). As the pioneering work Margerin et al. [22] showed that the late coda can be considered to be in the diffuse field regime after sufficient lapse time from the onset of S-wave. Then the idea is extended by Kawase et al. [23] to the stack of Horizontal-to-Vertical ratios of earthquakes (EHVR) and provide a simple theoretical formula assuming equipartition of energy in the incident waves at the bedrock (i.e., equipartition inside the half-space). It turned out that this is a powerful tool to determine the S-wave velocity structure below the observed site of earthquakes down to the seismological bedrock, as evidenced by subsequent papers [24–26].

Before the advent of application of DFC to EHVRs as mentioned above, the same concept is applied to the Horizontal-to-Vertical ratios of microtremors (MHVR) to derive a formula with horizontal and vertical Green's functions of a point force on the surface [27]. This theoretical formula may provide the final solution for the long-lasting debate on the interpretation of MHVR [28–31] started from the initial proposal by Nakamura [32]. The validation studies of this DFC interpretation of MHVR can be found in the recent studies [33–35]. More recently a new scheme of calculation using the residue integral is shown [36], which is much more efficient in computation of Green's functions and so can be used for velocity inversion.

We should recall at this point that the initial proposal by Nakamura [32] was to use MHVR as a direct substitute of the S-wave amplification factor of earthquake in the horizontal component, that is, Horizontal-to-Horizontal spectral ratio (HHR) of FAS with respect to the bedrock input. In his original proposal MHVR and EHVR were not strictly distinguished and therefore basically MHVR was assumed to be the same

as EHVR. As shown in Sánchez-Sesma et al. [27] for MHVR and Kawase et al. [23] for EHVR based on the DFC interpretation, it should be different from each other since the predominant incident wave types are different. As observed evidence there are more reports that do not support the idea of their similarity [e.g., 37,38] than those that support. However, systematic comparisons between EHVRs and MHVRs had not been made until Mori et al. [39] have studied from a practical view point of S-wave velocity inversion by using the transformed version of MHVRs.

Their motivation is to propose an empirical method in which translation from MHVR to EHVR is performed based on the averaged spectral ratio between EHVR and MHVR, which is called here as EMR. Once EMRs are calculated for different categories classified based on their fundamental peak frequencies in MHVR, f_{peak}, it is proved that the transformed HVR from MHVR, called pseudo EHVR or simply pEHVR, shows quite similar characteristics to the observed EHVR. Since it is much more efficient to invert a velocity structure from EHVR than MHVR thanks to its simple 1-D transfer function formula [23], it is practically useful to use pEHVR as a substitute to observed EHVR [39]. However, our motivation here to use EMR is to transform MHVR into EHVR since our goal is to obtain empirically the S-wave amplification factors of earthquakes.

Finally, we need to correct effects of vertical component amplification as Vertical-to-Vertical spectral ratios (VVR) of FAS, which is also neglected (that is, assumed to be 1.0) in the original Nakamura's formulation [32]. Because of the non-negligible amplification in the vertical component on the surface sensors, several articles that compared observed amplitudes of EHVRs with observed or theoretical amplitudes of HHRs at the same sites reported that EHVRs tend to underestimate HHRs, especially in higher frequency range [e.g., 18,40,41], although there are a couple of papers that showed that EHVRs closely correspond to HHRs [e.g., 38]. Since EHVR is the result of the ratios of transfer functions for a vertically incident S-wave with respect to a vertically incident P-wave under DFC interpretation, we need to correct P-wave amplification factor to obtain HHR from EHVR. Please note that this P-wave amplification is due to the incident vertical component of S-wave so that observed VVRs should be calculated from the vertical component of the S-wave part, not from the P-wave part (although their VVRs are quite similar). In this study we calculated the average VVRs determined by GIT reported in [15,16] using the same site categories used in EMRs for averaging operation.

As for the spectral ratio between the horizontal and vertical components at the bedrock, which was again assumed to be 1.0 in the original Nakamura method [32], it is implicitly included in the spectral ratios from GIT, since we used the same constraint for both the horizontal and vertical components at the reference site. Detailed description will follow.

2. Method and data

2.1. Earthquake data for EHVR

After the 1995 Hyogo-ken Nanbu (Kobe) earthquake, several nationwide strong ground motion observation networks have been deployed in Japan and we used here K-NET [42] and KiK-net [43,44] stations for earthquake ground motions, operated and distributed by National Research Institute for Earth Science and Disaster Resilience (NIED). Among these K-NET and KiK-net measurement sites, which is around 1600 sites in total, we observed microtremors (ambient noises) at 100 points by our own efforts from 2000 to 2015. The locations of the sites considered in this study are shown in Fig. 1 [39].

For earthquake ground motions first we select the earthquake data from the database provided by NIED, which contains source information determined by Japan Meteorological Agency (JMA). Then we cut out an S-wave record section from the observed data based on the S-wave onset calculated from JMA's source information and the travel time table (the so-called JMA2001 table, JMA, 2001). The duration of each record section is fixed to be 40.96 s. We also cut out another successive 40.96 s record section as a coda part to compare its spectral characteristics to the S-wave part. After the extraction of these two record sections we calculate their FAS and then take a spectral ratio of root-mean-square (RMS) values of two horizontal components with respect to the vertical component to obtain EHVR. Once all the records are analyzed then we calculate the average of all the EHVRs to obtain the average and the average ± one standard deviations.

In this research we analyzed earthquake motions with PGA from 1.0 to 50.0×10^{-2} m/s^2 among retrieved earthquake records. This is because the S-wave may not be clear in seismic motion records if PGA is less than 1.0×10^{-2} m/s^2 and earthquake records exceeding 50.0×10^{-2} m/s^2 may show nonlinear behavior of the underground structure [45]. Moreover, seismic motions of earthquakes exceeding the JMA magnitude M_{JMA} 6.5 is excluded from analysis to remove earthquake records with significant long period components predominantly due to basin-induced surface waves.

The portion before the arrival of P-wave is considered as a noise part and used to calculate signal-to-noise ratios. Records with duration less than 40.96 s are padded with zeros at the end. A cosine-shaped taper is added to both ends before the Fast Fourier Transform (FFT). Its length is set to be 10% of the data length for the noise part and 2.0 s for the S-wave and coda parts.

The time history waveforms of three components, namely, north-south (NS), east-west (EW), and up-down (UD), are transformed into the frequency domain by FFT to get FAS. Spectra of earthquakes where the signal-to-noise ratio is 2 or more are used to calculate average EHVRs. Before taking the ratios three components of FAS are smoothed using a 0.1 Hz Parzen window.

The individual spectral ratios of NS/UD and EW/UD showed a good match as a whole, although there are a couple of sites that showed difference in amplitude more than twice (or half) around f_{peak}. This kind of directional dependence suggests the effect of 2D/3D surface topography or irregularity in the basin structure [46]. Since we are taking the RMS horizontal amplitude to obtain EHVR, the influence of the directional dependence would be minimal. Fig. 2 shows the EHVRs of each observed earthquake and the average EHVR at EHM012 as an example. Please note that spectra higher than 30 Hz at K-NET sites are under the influence of their anti-alias filter. The black lines are the individual EHVRs (RMS/UD) of earthquakes and the gray line is their average. We can see that the EHVRs of individual earthquakes share the common shape, and the average EHVRs of both the S-wave part and the coda part are quite similar to each other. The latter phenomenon was already reported in [47] for about ten sites in the Sendai basin. It should be noted, however, the deviation from earthquake to earthquake is larger in the coda part, especially in the low-frequency range. The coda part is considered to be stable in amplitude because of multiple scattering with different directions of arrivals, but the S-wave part is found to be as stable as or more stable than the coda part in terms of the HVRs.

2.2. Microtremor data for MHVR

For measured microtremor records first the whole continuously observed records with 900–1200 s in duration are subdivided into record sections of 40.96 s by overlapping 50%. Then all the time history waveforms are visually inspected and fifteen best segments are extracted that are less affected by the local, time-varying noises.

As is the earthquake data analysis, three components are used for analysis, horizontal components of which are used to calculate their RMS value. Then MHVR is calculated as a ratio of RMS/UD. Finally, MHVRs calculated for each segment are averaged over fifteen segments. Smoothing on the Fourier spectra is obtained by 0.1 Hz Parzen window as in the earthquake analysis. Also a cosine taper of 2.0 s is added to both ends of the time history before FFT.

There is not so much difference between NS/UD and EW/UD of each

Fig. 1. Location of measurement points [39].

site, as is the case of earthquake motions. Fig. 3 shows the MHVRs of individual segments (RMS component, black lines) and the averaged MHVR (gray line) at the site EHM012 as an example. As is well known, the MHVRs are quite stable with time.

2.3. DFC theory for EHVR

We summarize basic formulas to calculate theoretical EHVR based on DFC. Under the assumption of DFC and subsequent energy-equipartitioned condition, we can show that the diffused-wave energy spectra $E(P, \omega)$ at the position P would be proportional to the normalized autocorrelation of observed displacement $|u(P, \omega)|^2$, which in turn would be proportional to the imaginary part of the Green's function at P as

$$E(P, \omega) \propto \left\langle \frac{|u(P, \omega)|^2}{\int |u(P, \varpi)|^2 d\varpi} \right\rangle \propto \mathrm{Im}(G(P, P, \omega)) \tag{1}$$

For EHVR coming from a far-field source, following [48], we can write

$$\left\langle \frac{|u(P, \omega)|^2}{\int |u(P, \varpi)|^2 d\varpi} \right\rangle = K \times |TF(\omega)|^2 = -K \times \rho_H c_H \omega \mathrm{Im}[G^{Eq}(P, P, \omega)] \tag{2}$$

where $\rho_H c_H$ is the impedance of the half-space, $TF(\omega)$is the transfer function of the corresponding body wave, G^{Eq} represents the Green's function for seismic source, ω is the circular frequency, and K is a constant. Therefore, we can get a simple formula for the surface observation (z = 0) of seismic motions as

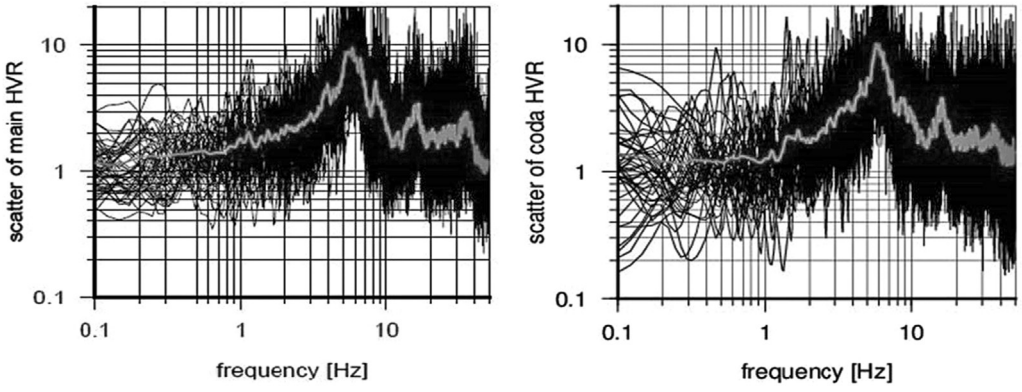

Fig. 2. Example of EHVR at a K-NET site EHM012. Left: S-wave part, right: S-coda part. Gray lines are the averages used for analysis.

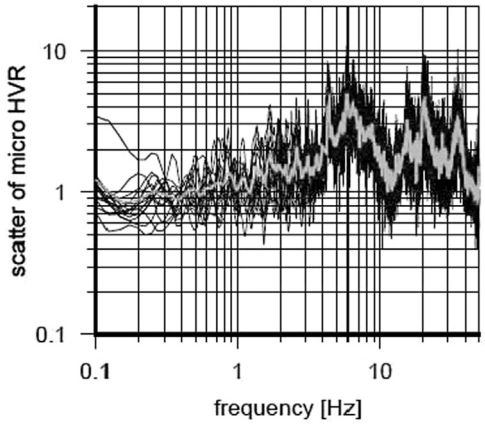

Fig. 3. Example of MHVR at a K-NET site EHM012. The gray line is the average used for analysis.

$$\frac{H(0,\omega)}{V(0,\omega)} = \sqrt{\frac{\mathrm{Im}[G^{Eq}_{horizontal}(0,0;\omega)]}{\mathrm{Im}[G^{Eq}_{vertical}(0,0;\omega)]}} = \sqrt{\frac{\alpha_H}{\beta_H}}\frac{|TF_{horizontal}(0,\omega)|}{|TF_{vertical}(0,\omega)|} \quad (3)$$

where $\alpha_H$and β_H is the P- and S-wave velocity of the half-space, respectively. In this case directional HVR (i.e., NS/UD and EW/UD) calculation is assumed [46].

Here we should emphasize the importance to consider the whole basin structure down to the seismological bedrock in EHVR. As shown here, EHVR depends on the equipartitioned energy ratios at the seismological bedrock, α_H/β_H, and the transfer functions of P- and S-waves from there to the surface. This means that even in a high frequency range EHVR would be a function of the deep basin structure, not only a function of shallower sediments above the engineering bedrock. To show the effects of a deep basin structure on EHVR in the high frequency range we plot results of a parametric study in Fig. 4. We use the best-fit model with 14 layers as a reference for MYG006 [25] and omit two layers in each step from the bottom of the reference model. As the bottommost P- and S-wave velocities decrease, the peak in the lower frequency range disappear, as expected. However, not as expected, the peak and trough amplitudes in the higher frequency range increase strongly at the same time. This means that not only the shallow sedimentary layers down to the engineering bedrock but also the deeper part down to the bedrock contribute to EHVR even in the high frequency range. In another words, when we use EHVR to evaluate the site amplification factor, the resultant factor would be the one from the seismological bedrock.

2.4. VVR evaluation

For the VVR evaluation for the S-wave portions of the observed earthquake records, we follow the implementation of GIT described in [15,16]. We only briefly describe the basic aspect of their analysis.

We used Fourier acceleration spectra (FAS) of strong ground motions observed by K-NET, KiK-net, and JMA Shindokei Network in Japan to separate source, path, and site factors based on GIT. The separation method that we used here is the same method proposed by Kawase and Matsuo [15] and used by Nakano et al. [16]. We include all sources larger than M_{JMA}4.5 observed from 1996 to 2011.

We limited earthquakes with source depth D $\leq$ 60 km and hypocentral distance from earthquake i to site j Xij $\leq$ 200 km, and records with PGA $\leq$ 2 m/s^2 to avoid deviation by site nonlinearity. We use only surface data for KiK-net because it would be redundant to use both surface and borehole data at the same location (except for the relative amplification between them, which can be obtained easily after the inversion). Selection using these criteria resulted in analysis of 972 K-NET sites, 601 KiK-net sites, and 532 JMA Shindokei Network sites, 2105 sites in total. The data covered 967 events with 446 subducting plate-boundary (type B) events, 294 subducting intraplate (type I) events, and 227 crustal (type C) events. There were 77,213 earthquake–station pairs. Fig. 5 shows magnitude-distance distribution of the used data for three different types of earthquakes with two categories of their source depths.

We used the horizontal component of YMGH01 for constraint where we can reasonably assume that no site effect would exist after correcting the theoretical site amplification from the bedrock (with S-wave velocity of 3.45 km/s) to the surface. We checked site factors for other hard-rock sites and found that the corrected YMGH01 shows actually the lowest and most stable (with respect to the frequency) characteristics among them.

In Fig. 6 we show the amplification factor of the vertical component at YMGH01 with respect to the horizontal component assumed as an outcrop motion of the seismological bedrock, V_bH_bR. When we compare this amplification factor with the theoretical prediction based on DFC from Eq. (3),

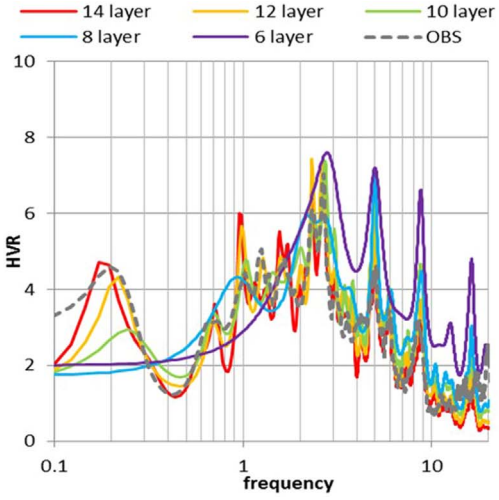

No.	Vs [m/s]	Vp [m/s]	H [m]	Depth [m]	Density [g/cm3]
1	42	709	2	2	1.54
2	64	756	2	4	1.57
3	116	865	3	7	1.63
4	128	891	5	12	1.64
5	257	1158	29	40	1.74
6	324	1296	34	74	1.78
7	464	1576	43	117	1.86
8	639	1916	502	619	1.94
9	872	2350	125	744	2.03
10	1133	2813	91	835	2.11
11	1593	3564	662	1497	2.25
12	2006	4171	238	1735	2.35
13	2404	4695	1245	2980	2.44
14	3400	5744	0	2980	2.64

Fig. 4. Comparison of 1D theoretical EHVRs for the velocity model identified at MYG006 (right-hand side table) with different numbers of layers from the top as a parametric study. The inverted structure has 14 layers down to the seismological bedrock and bottommost two layers are excluded in a stepwise manner to create shallower layered models until 6 layers. We should note that the less numbers of layers make different EHVR even in the high frequency range. This is because high frequency EHVR is influenced by not only amplification due to shallow soft layers but also amplification of higher modes (i.e., reverberations within the whole layers down to the bedrock).

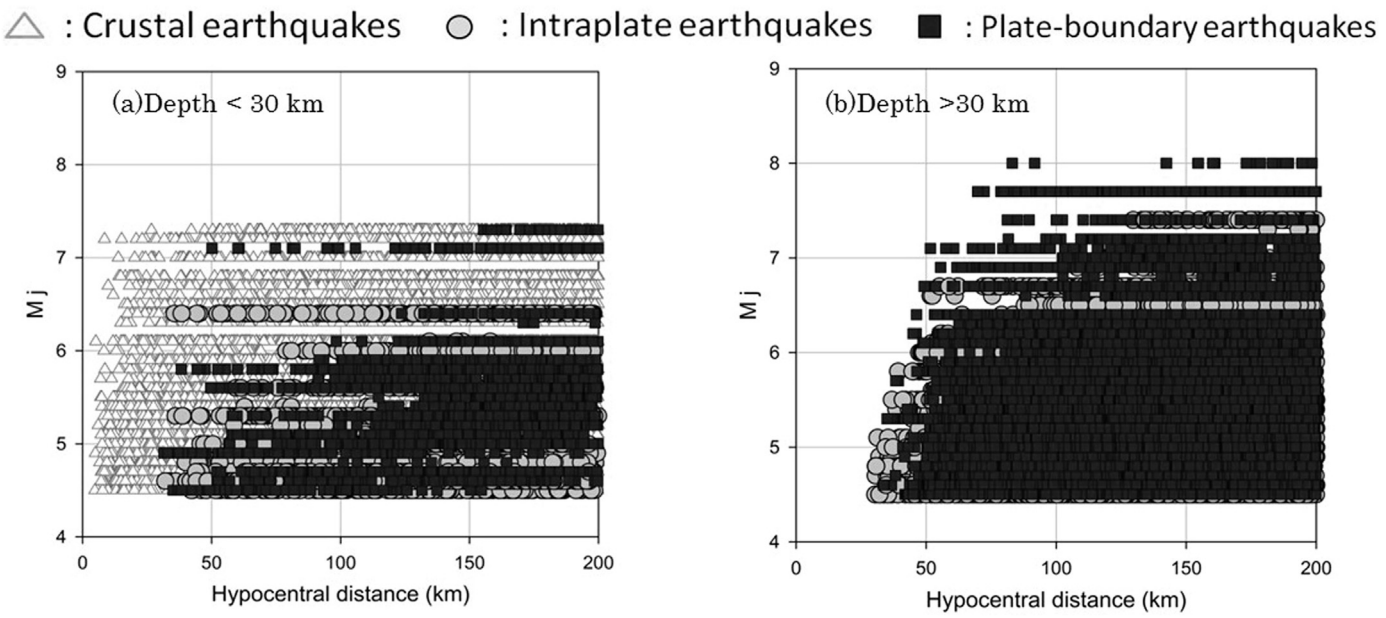

Fig. 5. JMA magnitude versus hypocentral distance distributions of all the used data with source depths (a) shallower than 30 km or (b) equal to/deeper than 30 km. Three different types of sources are distinguished in GIT [15,16] but the same site amplification is assumed.

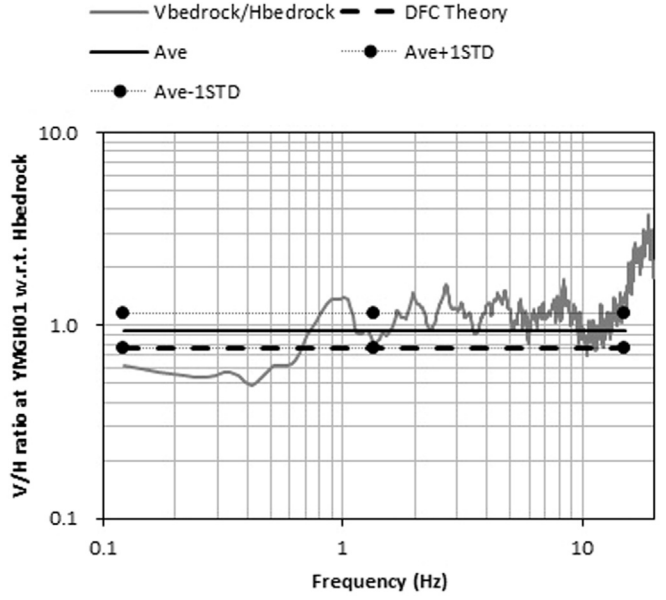

Fig. 6. The resultant V_bH_bR at the reference station YMGH01 as input motion on the outcrop of the seismological bedrock and its frequency average and average + /- one standard deviation, together with the theoretical value predicted from DFC.

$$V_bH_bR = \frac{V_{bedrock}(0,\omega)}{H_{bedrock}(0,\omega)} = \sqrt{\frac{\beta_H}{\alpha_H}} \tag{4}$$

which would be a frequency independent value of 0.76 if the bedrock (as a half-space) would be a Poisson solid. It is very close to the lower bound of the average and the average minus one standard deviation as shown in Fig. 6. The fluctuation with respect to frequency is about ± 30%.

Please note that the observed horizontal component at YMGH01 is corrected by the one-dimensional S-wave theoretical amplification factors based on the inverted velocity structure because of the significant influence of the weathered layers as mentioned above, while the vertical component for P-wave amplification is not corrected. So we can see significant amplification in the vertical component at YMGH01 in the frequency range higher than 15 Hz probably due to the P-wave velocity contrast in the weathered layers. As shown below, we will actually not use vertical-to-vertical ratios in this study but vertical-to-horizontal bedrock input ratios so that neglected amplification for the vertical component at the reference site is carried over to the estimated vertical amplification. Because of this obvious amplification in the frequency range higher than 15 Hz in V_bH_bR, we need to restrict the frequency range of reasonable prediction of HHR up to 15 Hz, although our calculations hereafter are covered up to 20 Hz.

Here we show basic theoretical background to get the S-wave amplification factor directly from VVR separated through GIT [15,16]. Suppose we have both the horizontal observed FAS on the surface of the sedimentary layer, *H_s*, at a target site and that on the surface of the seismological bedrock, *H_b*, at the reference site. The site amplification factor HH_bR (as a function of frequency f) for the horizontal component at the target site can be defined as:

$$HH_bR = H\_s/H\_b \tag{5}$$

Hereafter only subscript b for bedrock motion is used in the ratio and HH_bR can also be described as HHR for brevity as long as it is not confusing (the same rule is applied to VVR for VV_bR). Then if we have both HVR of earthquakes at the target site, that is EHVR,

$$EHVR = H\_s/V\_s \tag{6}$$

and VV_bR between the target site and the reference site,

$$VV_bR = V\_s/V\_b \tag{7}$$

then HH_bR can be obtained by

$$HH_bR = EHVR^*VV_bR^* \quad V_bH_bR \tag{8}$$

where V_bH_bR is the vertical-to-horizontal spectral ratio at the reference site shown in Eq. (4) and Fig. 6, which is

$$V_bH_bR = V\_b/H\_b \tag{9}$$

using the similar notation. Eq. (8) is obvious because

$$HH_bR = H\_s/H\_b = (H\_s/V\_s) \quad ^*(V\_s/V\_b)^*(V\_b/H\_b) \tag{10}$$

In our actual implementation based on the GIT with respect to the common horizontal bedrock motion at the reference site [15,16] we have relative amplification ratios of the vertical component spectra at a target site with respect to the horizontal bedrock input motion, that is,

$$VH_bR = V\_s/H\_b \quad (11)$$

So we can get HH_bR through

$$HH_bR = EHVR*VH_bR \quad (12)$$

Since this equation is nothing but a tautology, we replace EHVR with EMR times MHVR, that is the pseudo EHVR, as:

$$pHH_bR = EMR*MHVR*VH_bR \quad (13)$$

where pHH_bR means the pseudo HH_bR. For actual prediction of the site amplification factor at a target site we need to use average values of EMR and VH_bR determined empirically before the prediction. If we name the empirical VH_bR as pVH_bR, then the final formula of prediction would be:

$$pHH_bR = EMR*MHVR*pVH_bR \quad (14)$$

This formula shows clearly the reason where the name of the proposed method, "double empirical correction method", comes from. Because they are also site dependent in a strict sense, precise prediction is difficult without the detailed information on the velocity structure. Thus the validity of the above simple formula (14) depends on the levels of inevitable variation in both EMR and VH_bR from site to site.

3. Results

3.1. EHVR and MHVR

Fig. 7 shows comparisons of EHVRs and MHVRs at six selected sites as examples. As pointed out before, EHVRs of the S-wave part and those of the S-coda part match each other at most of the sites. On the other hand comparison of EHVRs of either the S-wave parts or S-coda part to MHVRs in between 0.2 and 20 Hz shows a notable difference between them; the EHVR amplitude after the fundamental peak (more precisely, after the first dip immediately after the fundamental peak) tends to be much larger than that of the MHVR and sometimes has several clear peaks after the first one, while the MHVR amplitude tends to be smoothly varying in these higher frequencies. This kind of difference is exactly what we should expect due to the different nature of wave field for microtremors and earthquakes. We can see that they are very close to each other as for the amplitude and the frequency of the first peak, as pointed out in previous studies such as [47].

3.2. Empirical EMR

The comparisons between EHVRs and MHVRs show that they are more or less similar until the fundamental peak frequency (f_{peak}) but that they are significantly different in the frequency range higher than that. Therefore, a way to extract statistically significant trend in the difference between EHVR and MHVR is proposed [39]. We calculated the earthquake-microtremor ratio, EMR, the ratio of the average EHVR with respect to the average MHVR for each site.

When we look at the spectral comparison for individual sites as in Fig. 7, we can see clear frequency characteristics in the difference between EHVR and MHVR as mentioned before. Assuming that f_{peak} of EHVR and MHVR is basically the same, which should reflect the specific velocity structure at that site, we can expect similar spectral characteristics in the EMRs for sites with similar f_{peak}. This is so because EMRs are expected to be the direct consequence of the wave field difference of earthquake and microtremor ground motions in the same velocity structure underneath.

Therefore, the average EMR for a normalized frequency with respect to f_{peak} (i.e., $f_{norm} = f/fpeak$) is derived by reading f_{peak} of MHVR. To suppress some spurious peaks we use a 0.3 Hz Parzen window on MHVR when we read f_{peak}, although average operation is performed for the data with 0.1 Hz Parzen window. From a practical view point, we

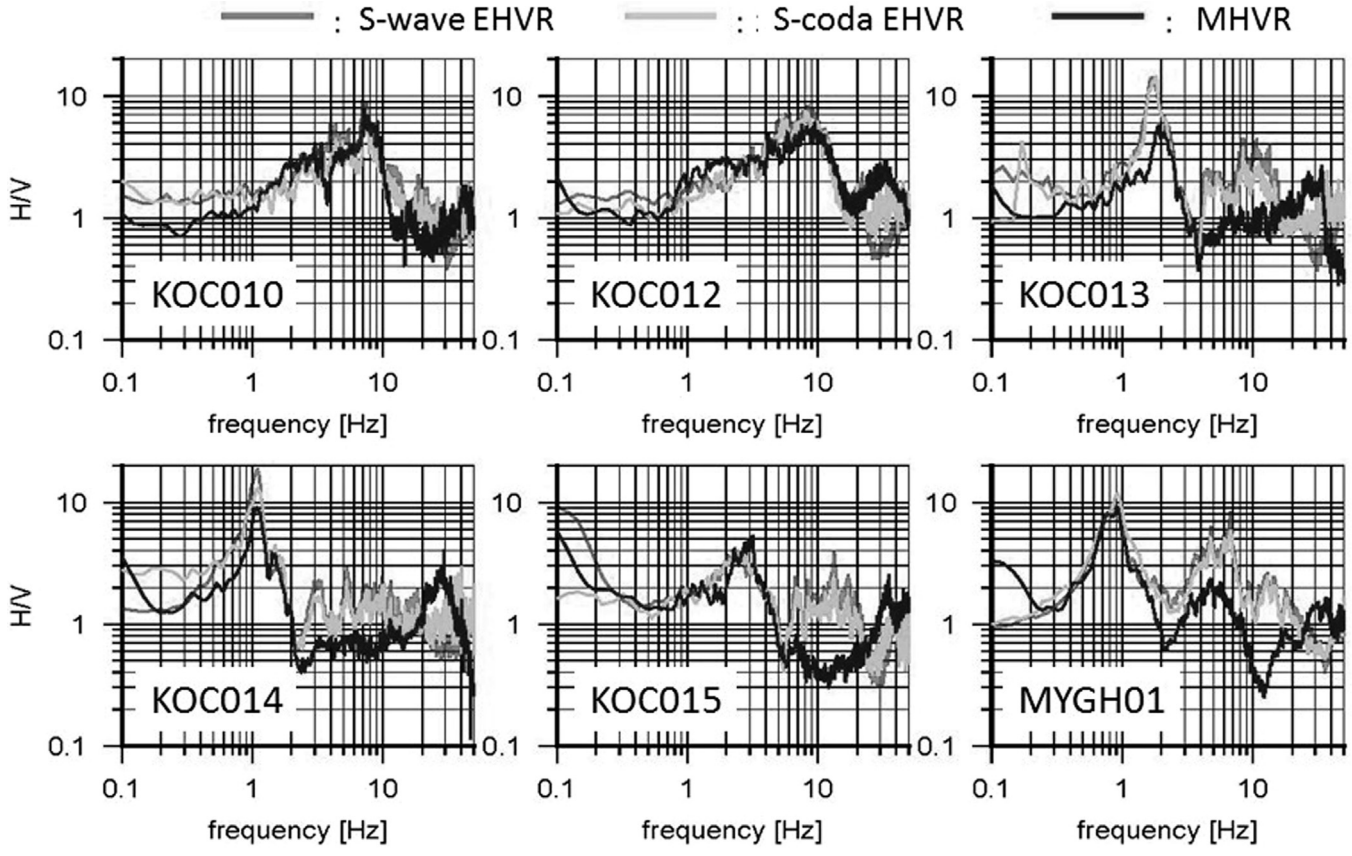

Fig. 7. Comparisons of EHVRs and MHVRs at six selected sites as examples. Dark gray lines are EHVRs of the S-wave part, while light gray lines are those of the S-coda part. Black lines are MHVRs.

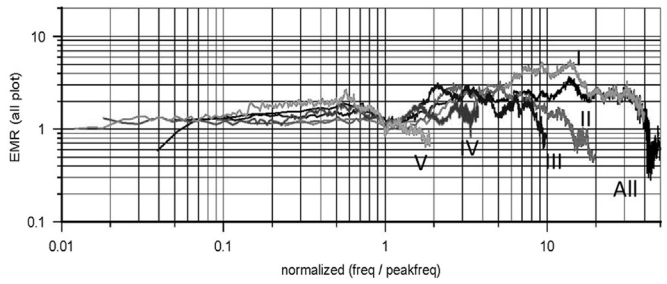

Fig. 8. EMR, the ratios of EHVR to MHVR, averaged over different fundamental peak frequency ranges of MHVR. Category I: 0.2–1.0 Hz, II: 1–2 Hz, III: 2–5 Hz, IV: 5–10 Hz, and V: 10–20 Hz. The horizontal axis is a normalized frequency with respect to the fundamental peak frequency of MHVR. A long black line is the averaged value for the whole frequency range from 0.2 to 20 Hz. We can see that significant correction factors are needed in the normalized frequency range higher than 2 for Category I to Category III.

would like to restrict EMR calculations for sites with a clear peak in between 0.2 and 20 Hz, so sites with MHVRs whose f_{peak} is less than 2 in amplitude or whose f_{peak} is outside of this range are excluded from further analysis. As a result, 87 sites are selected for averaging operation to get normalized EMRs.

When we calculate EMRs for these 87 sites, it is apparent that the normalized frequency range is going into very low frequency and sampling is quite dense when f_{peak} is high ($>$ 10 Hz), while it is going into high frequency and sampling is very sparse when f_{peak} is low ($<$ 1.0 Hz). Also it would be more physical to have different correction factors depending on f_{peak} since it reflects physical amplification characteristics at the site. Therefore, the sites are categorized based on f_{peak} and the average EMRs are calculated for five categories. Fig. 8 shows the average frequency-normalized EMRs in five f_{peak} categories, namely 0.2–1 Hz, 1–2 Hz, 2–5 Hz, 5–10 Hz, and 10–20 Hz. We may get a smaller variation if we use a smaller frequency range but then the reliability of the average EMR will be decreased since the number of the sites in one category will be decreased. As the numbers of available sites increase, the numbers of categories used may increase in future.

In Fig. 8 distinctive features are evident in different categories. Most notably, the amplitude of EMR after f_{peak} (precisely speaking, when $f_{norm} \geqq 2.0$, which means after the first dip) is especially large when f_{peak} is in between 0.2 and 5 Hz (i.e., Category I to III). In Fig. 8 we also shows the whole average EMR without considering category. The average EMRs in adjacent categories show a similar amplitude in the frequency range with overlapping, but they are not exactly the same, especially when f_{norm} is in between 2 and 10. This means that average EMRs calculated in these five categories here should be used for better representation of EMRs, not the EMR without category.

3.3. Validity of pEHVR

Once we obtained the average empirical EMRs, we can transform MHVRs into pseudo EHVRs, or simply pEHVRs. To see the validity of the EMR correction, we plot comparisons of EHVR, MHVR, and pEHVR in Fig. 9 for one representative site from each category. As we can see, correction by EMR to MHVR is quite effective to reproduce EHVRs for most of the sites. We compared frequency correlations between MHVR and EHVR and between pEHVR and EHVR to see significant improvement in the latter, especially sites with higher peak amplitude in MHVRs. Thus EMR correction is meaningful to make MHVR closer to EHVR.

3.4. Empirical VH_bR

Following the EMR correction we also calculated VH_bR, amplification of the vertical component at a target site relative to the horizontal bedrock input and then calculate average for the same group of sites (i.e., categories) as used in the EMR correction factors. Because we prefer classifications of sites solely based on the microtremor measurement at the target site, we use the same category depending on f_{peak} of MHVR.

Because of the dependency of VH_bR on the P-wave velocity structure underneath at the target site, we may also use the site category based on the fundamental peak frequency of the vertical-to-horizontal spectral ratio of microtremor, MVHR, which is nothing but the inverse of MHVR, in order to give more emphasis on the peak frequency in the vertical component. However, since the frequency ratio between the fundamental peak frequency in the horizontal component and that in the vertical component (that is the dip frequency in MHVR) is quite stable for sediment sites [49–51], the use of f_{peak} in MHVR can be a simple but rational choice.

Before looking into VH_bR for empirical correction to get pseudo HH_bR, the pseudo horizontal-to-horizontal spectral ratios with respect to the bedrock motion, we would like to see average characteristics of the site factors in both horizontal and vertical components. Fig. 10 shows the average and average plus/minus one standard deviation of the site amplification factors in the horizontal and vertical components with respect to the horizontal (S-wave) bedrock motion, that is, HH_bR and VH_bR for all 100 sites used. Thin gray lines are individual values at arbitrarily selected sites as examples to show their variability. We can see HH_bR is much higher than VH_bR in the frequency range from 1 to 10 Hz. However, except for the amplitude difference of about 4 times, the averaged frequency characteristics with almost constant amplitude are quite similar to each other in the above frequency range. Please note that the peak at around 17 Hz in VH_bR is primarily due to the P-wave amplification at the reference site as already mentioned and shown in Fig. 6.

In Fig. 11 we show pseudo VH_bR, or simply pVH_bR for five categories, that is, the observed VH_bRs averaged over sites in each category depending on f_{peak}. The individual VH_bR of several sites used in the average are shown in Fig. 12 for Category I as an example. It is surprising that VH_bRs for sites with the same category are similar to each other so that it looks quite effective to replace real ratios with the averaged one. The difference between categories are also minor, although the difference between Category I, II, and III and Category IV and V seems significant in comparison to the standard deviation. Please note that we use real frequency in Hz for pVH_bR since it is not quite physical to normalize f_{peak} as in EMR.

3.5. Double empirical correction to MHVR

After we prepare both the microtremor to earthquake correction, EMR, and the vertical amplification correction, pVH_bR, we can check reproducibility of the observed S-wave site amplification factor derived from GIT, HH_bR, based on the double correction to MHVR as shown in Eq. (14).

Figs. 13 to 17 show five examples of comparison between pEHVR, pVH_bR, that is the averaged VH_bR, and pHH_bR = pEHVR*pVH_bR as in Eq. (14), together with the real HH_bR, for one representative site from each category. The comparison can be made with the same pEHVR, real VH_bR, and pHH_bR from the real VH_bR as in Eq. (13), together with the same real HH_bR, which are shown in the left-hand side panel. We can see that the direct comparison between pEHVR and the real HH_bR is not satisfactory at all for these examples, while the resultant doubly corrected pHH_bR is much closer to the observed HH_bR. Although it is not a perfect match, similarity of pHH_bR from the real VH_bR in the left-hand side panel is higher than that of pHH_bR from the empirical VH_bR in the right-hand side panel, which is natural since the empirical VH_bR is the averaged one over the sites in the same category.

4. Discussion

As mentioned above the degree of correction is almost the same for these two corrections so that we need to consider both corrections in

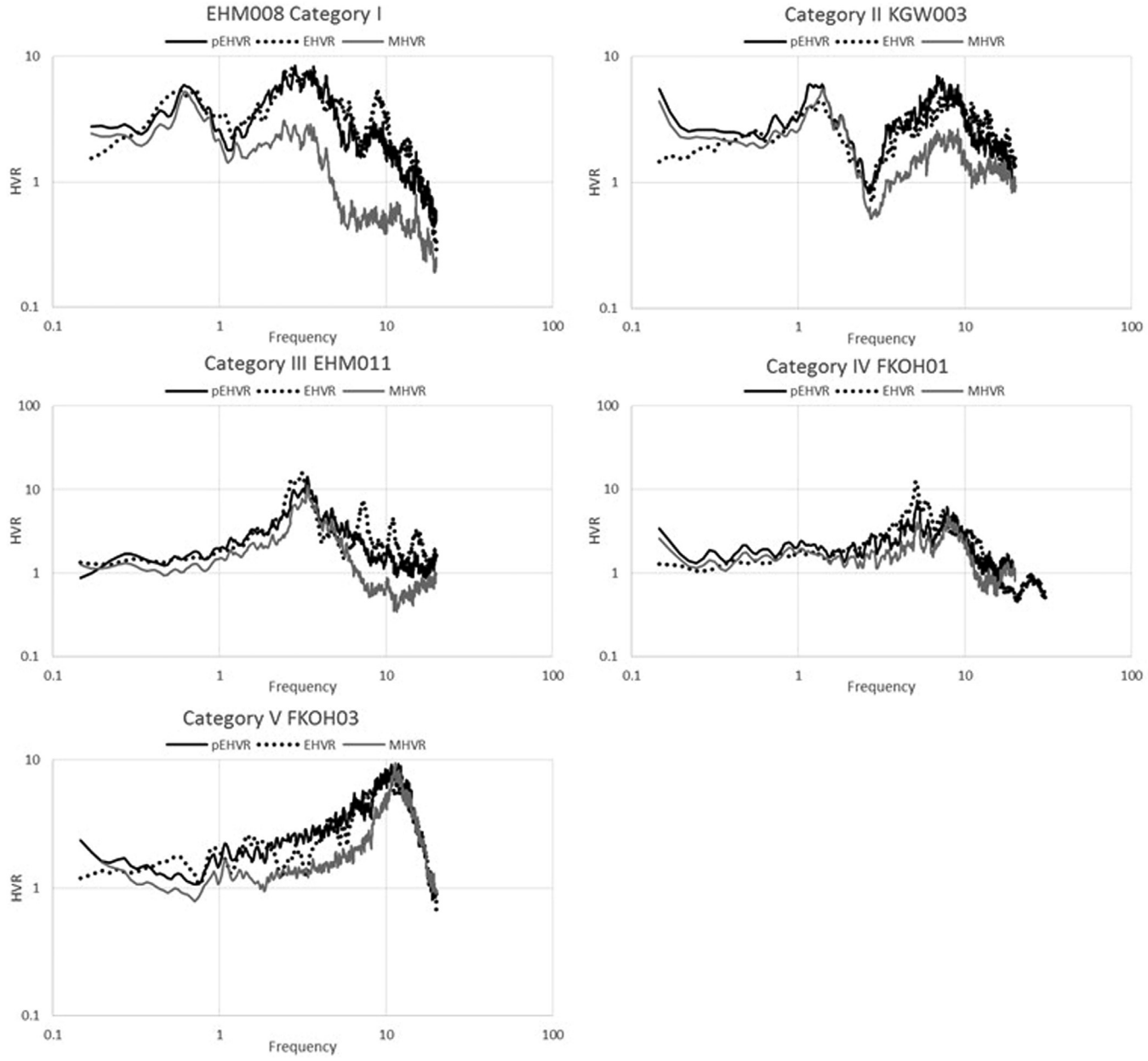

Fig. 9. Direct comparison of EHVRs of S-wave (dotted lines), MHVRs for microtremors (gray lines), and pEHVRs transformed from MHVR by using empirical EMR for each category (black). We can see significant shift of amplitude toward EHVR by using EMR correction proposed here.

order to transform MHVR into HH_bR with sufficient accuracy. The final difference in between pHH_bR and HH_bR is coming from the average operation in both EMR and VH_bR, although the differences of pHH_bRs in between left- and right-hand side panels in Figs. 13 to 17 show that the contribution from VH_bR may be slightly stronger than that from EMR.

To see overall matching we performed the double corrections onto all the 100 sites used in this study and compare the correlations and log-residuals with respect to frequency and ratios of frequency-weighted average amplitudes between pHH_bR and HH_bR. For sites with f_{peak} outside of the range from 0.2 to 20 Hz we substituted the correction factors in the nearest category. Fig. 18 shows correlations and residuals in logarithm (which means that we obtained the average ratios with respect to HH_bRs) while Fig. 19 shows ratios of the averaged amplitudes for 100 sites, both of which are sequentially listed in the horizontal axis. In the latter we also plot the ratios of pEHVR with respect to HH_bR as the starting point of the bar to grasp the effect of our pVH_bR correction. There are some sites where exceptionally large differences exist, namely, KOC015, TTR008, SMNH10, and SMNH11, however, in the overall comparison we can see the effect of the double correction, especially the effect of pVH_bR correction. Note that the averaged value of the residuals, 1.6, does not mean the pHH_bR tends to overestimate HH_bR. Rather the average difference (=ratio) between pHH_bR and HH_bR is in the range of 1.6 times or 1/1.6 times.

4.1. Validation at MYG015

So far the operation is circular in a sense except for the average operation in EMRs and pVH_bRs for each category based on f_{peak} of MHVR. We need independent evidence to support the validity of these empirical EMR and pVH_bR corrections for quantitative evaluation of site amplification factors. The validity of the empirical EMR correction has already been presented in Mori et al. [39] for six sites in Sendai, Japan. Unfortunately, five sites except for MYG015 are not included in

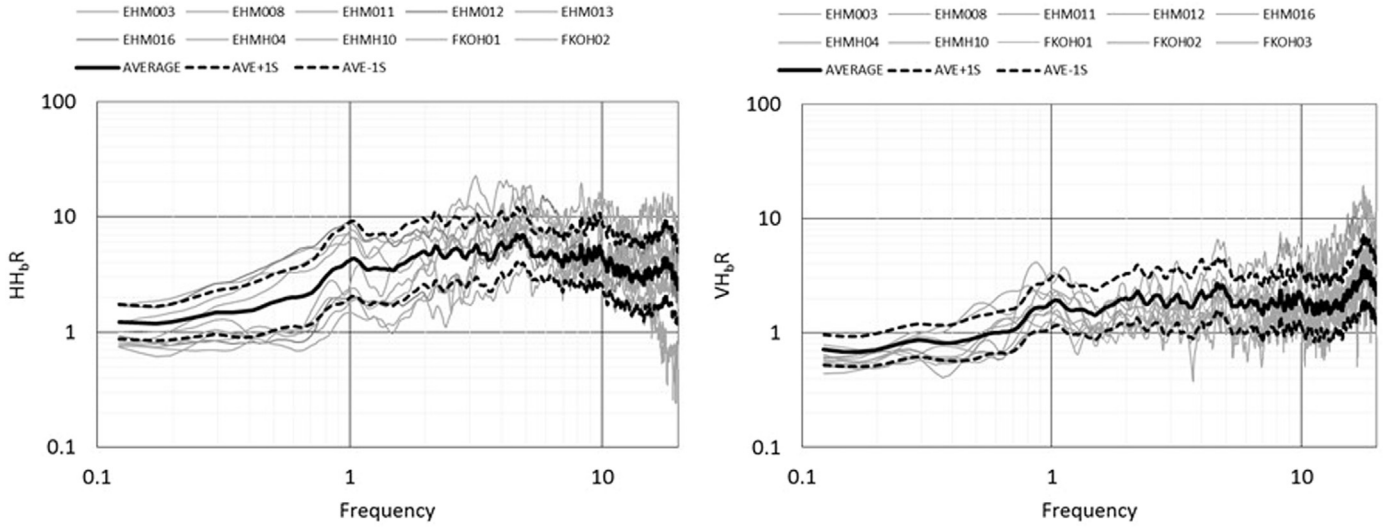

Fig. 10. The average and average plus/minus one standard deviation of HH_bR (left-hand side) and VH_bRs (right-hand side) for 100 sites used in this paper. In GIT used to get these amplification factors, the common reference of 1-D amplification corrected horizontal component at YMGH01 is used so that VH_bR in the right-hand side panel is actually the ratio of vertical component with the same reference of the horizontal bedrock motion as mentioned in the text. Note that peak in VH_bR in the frequency range higher than 15 Hz is probably due to P-wave amplification of weathered layers at the reference site, that is, V_bH_bR, shown in Fig. 6.

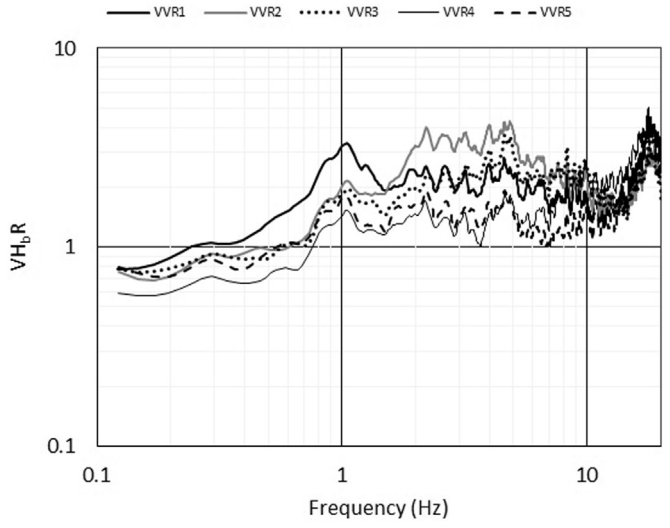

Fig. 11. Average VH_bRs categorized by the fundamental peak frequency in MHVR as in EMR, without frequency normalization. Peak frequencies for Category I to V tend to increase as the peak frequency ranges increase from 0.2 to 1 Hz (Category I) to 10–20 Hz (Category V). A prominent peak at 15 Hz common to all the category would come from the P-wave amplification due to weathered layers at the reference station, that is, V_bH_bR, shown in Fig. 6.

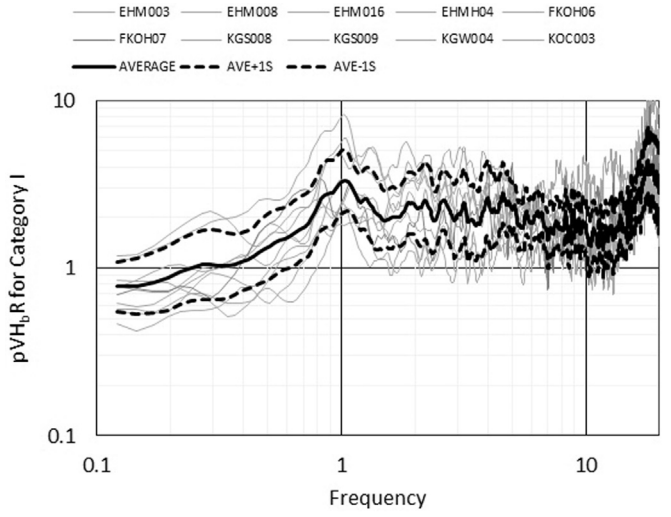

Fig. 12. The averaged pVH_bR for Category I and the individual VH_bR of several sites used in the average are shown in Fig. 12 as an example.

the database of strong motions used in [16] because these were the independent network deployed by BRI [46]. Thus we show below the comparison at only one K-NET site, MYG015 in Miyagi Prefecture, Tohoku, Japan, where we measured microtremors well before the 2011 M9.0 Tohoku earthquake [47].

Fig. 20 shows comparisons of pEHVR derived from MHVR, the real EHVR, and observed MHVR (up to 10 Hz because it was the target frequency range in [47]) at MYG015, and Fig. 21 shows pEHVR and pHH_bR from [pEHVR * VH_bR] in comparison to HH_bR in the left-hand side panel while pEHVR and pHH_bR from [pEHVR * pVH_bR] in comparison to HH_bR in the right-hand side panel. Comparing the observed ones with pseudo ones, namely, EHVR and pEHVR, and HH_bR and pHH_bR, we found that pEHVR from microtremors more or less matches EHVR but that pHH_bR from pVH_bR in the right-hand side panel underestimates HH_bR, primarily because of the amplitude deficiency in pVH_bR compared to the real VH_bR. This example shows again the importance of the vertical amplification correction when we refer to HVR to obtain an S-wave site amplification factor. Since we have not many independent observations of MHVRs at seismic stations where we have both HH_bR and VH_bR yet, quantitative validation of our proposed method will be the main theme of our future studies.

5. Conclusions

In this study we calculated horizontal-to-vertical spectral ratios (HVR) from observed microtremors (MHVR) as well as those of observed weak earthquake ground motions (EHVR) at the same site and calculated their ratios (EMR) because there should be a systematic difference based on the theory developed under diffuse wave concept. When we compared MHVRs and EHVRs at 100 strong motion observation sites in Japan, we found that their fundamental peak frequencies and their amplitudes (as well as the first dip frequencies) are remarkably similar to each other but there are significant differences in their amplitudes and frequency characteristics after the fundamental peak frequency (more precisely, after the first dip frequency adjacent to the fundamental peak frequency) in MHVR. This is because MHVR

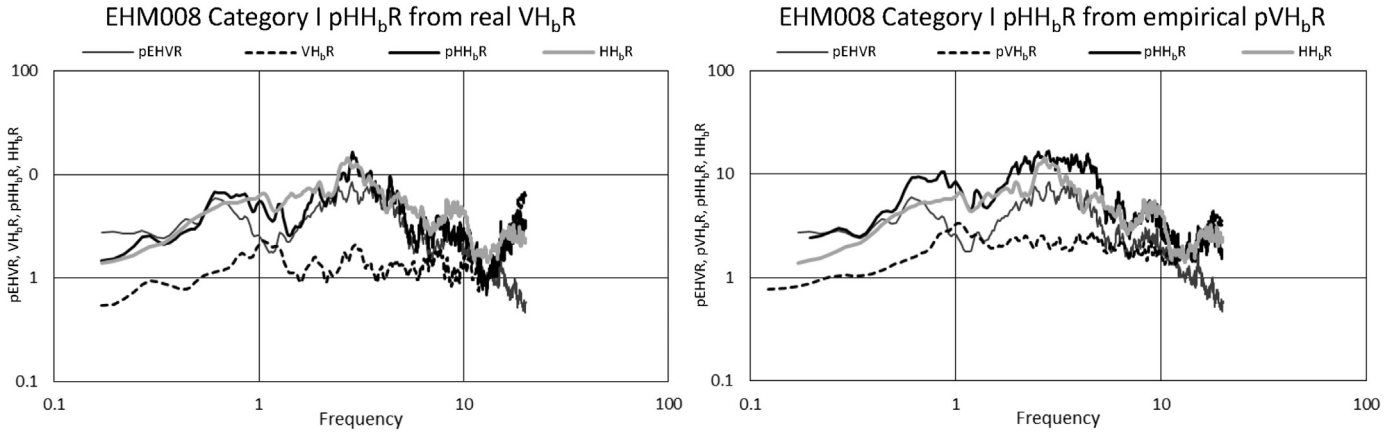

Fig. 13. pEHVR, the real VH_bR, and $pHH_bR = pEHVR*VH_bR$, in comparison to real HH_bR in the left-hand side panel and the same pEHVR, the averaged pVH_bR, and $pHH_bR = pEHVR*pVH_bR$, in comparison to real HH_bR for EHM008 in Category I. The difference between pHH_bR and HH_bR in the left-hand side panel and those in the right-hand side panel is due to the difference of the average operation in pVH_bR.

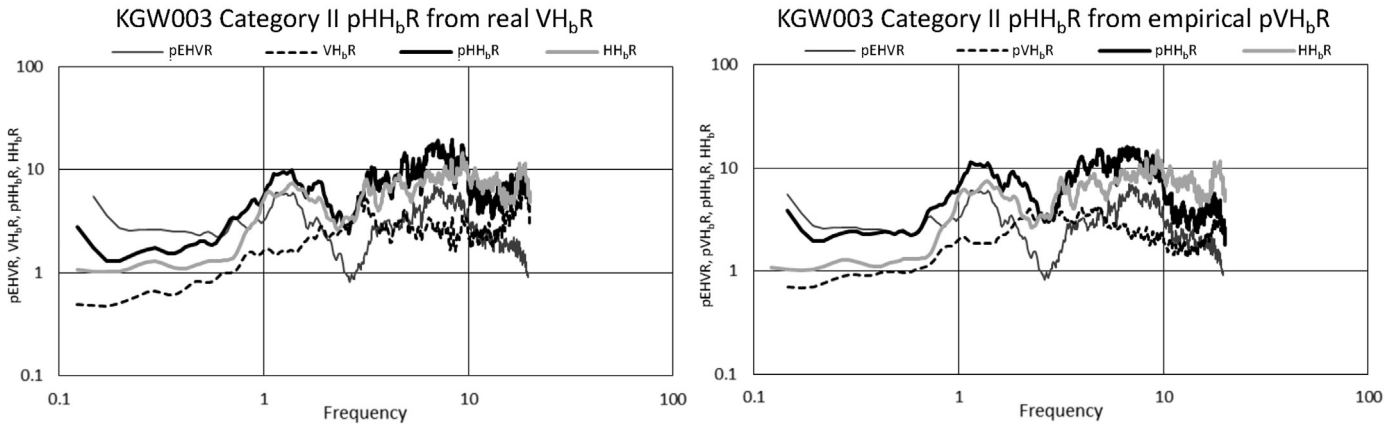

Fig. 14. The same comparison as Fig. 13 for sites Category II.

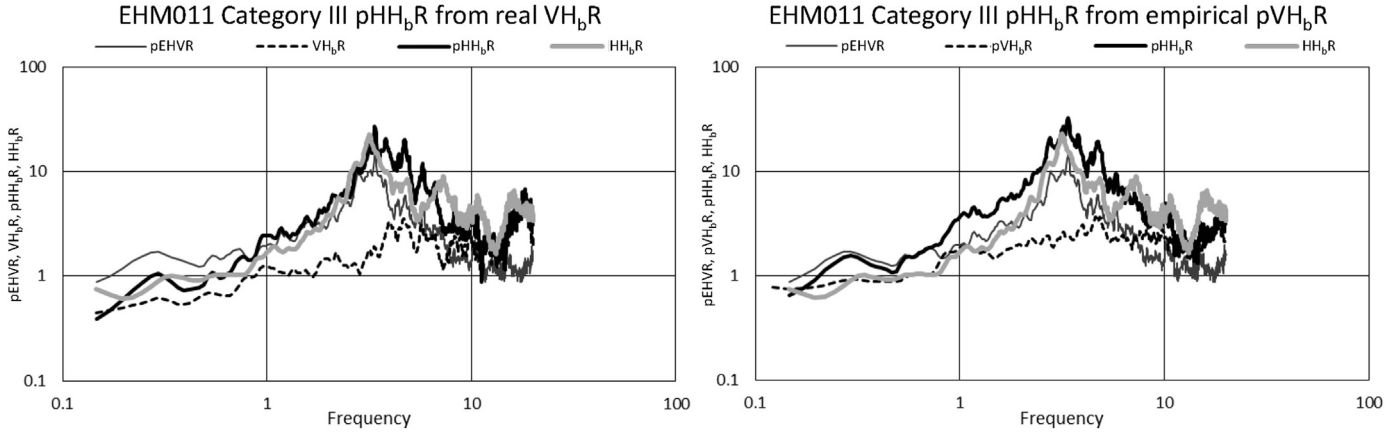

Fig. 15. The same comparison as Fig. 13 for sites Category III.

mainly consists of surface waves so that peaks associated with higher modes would not be so much excited as that of EHVR.

To fill the gap between MHVR and EHVR, we established an empirical correction method to obtain pseudo EHVR from MHVR by using EMRs at these 100 sites in Japan. We proposed to use EMRs, averaged over sites divided into five different categories based on the fundamental peak frequency (f_{peak}) ranges of MHVRs, as a function of the normalized frequency f/f_{peak}. We converted MHVRs into pseudo EHVRs by multiplying MHVRs with the average EMRs, which are found to have higher correlation with real EHVRs than MHVRs.

Once we obtained pEHVRs we can then transform pEHVRs into pHH_bR, that is, pseudo horizontal (S-wave) amplification factors with respect to the bedrock input in the horizontal direction, by correcting vertical-to-vertical spectral amplification from the bedrock to the surface (VV_bR). Precisely speaking, we need to correct not only VV_bR specific to the site but also V_bH_bR commonly seen at the bedrock, which is the relative amplitude correction between equipartitioned vertical (V_b) and horizontal (H_b) components on the outcrop of the seismological bedrock. Thanks to the natural procedure of the generalized spectral inversion for both horizontal and vertical components using

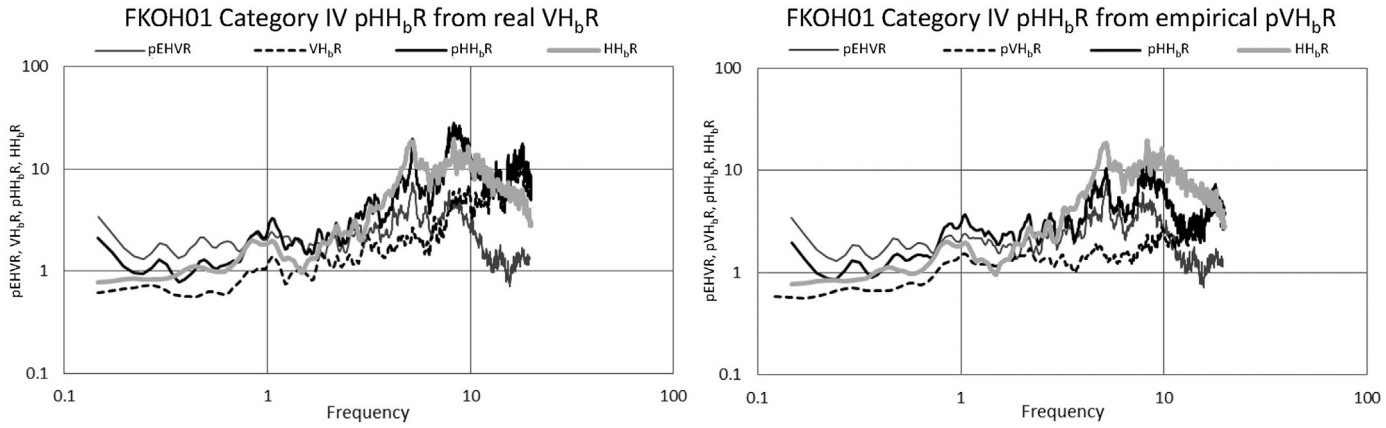

Fig. 16. The same comparison as Fig. 13 for sites Category IV.

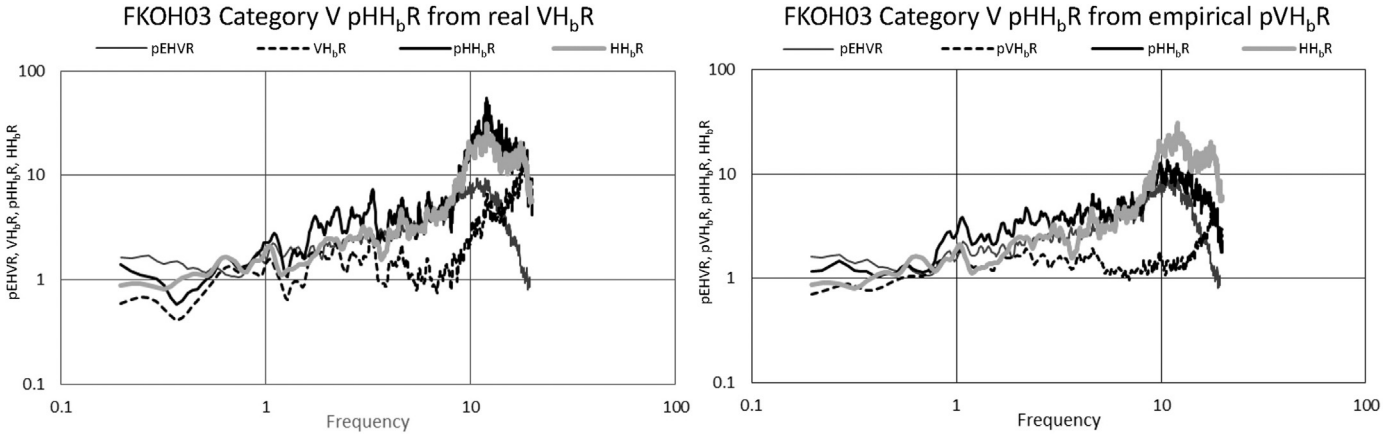

Fig. 17. The same comparison as Fig. 13 for sites Category V.

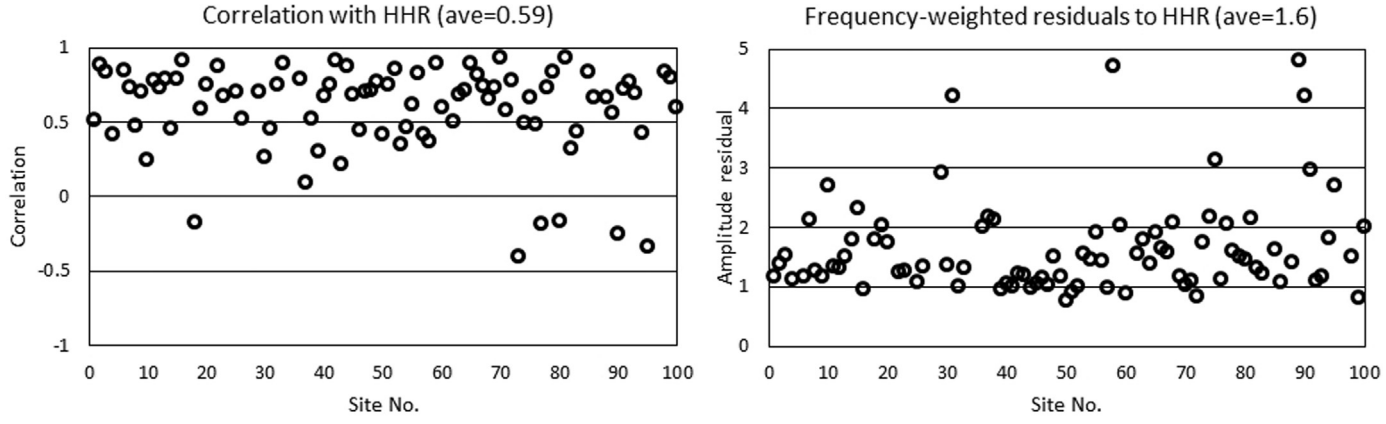

Fig. 18. Correlations and frequency-weighted average residuals in log (i.e., ratios) between pHH$_b$R and HH$_b$R for all the 100 sites, sequentially listed in the horizontal axis.

the same reference constraint, we obtained VH$_b$R at 100 sites, which corresponds to [VV$_b$R * V$_b$H$_b$R]. After looking at the basic spectral characteristics of VH$_b$Rs, we decided to propose empirical correction factors of VH$_b$R again as the averaged values over the sites with the same categories of f_{peak} as used for EMR, although no normalization is used. The resultant VH$_b$R correction factors are relatively similar to each other but there are significant differences between Category I to III and Category IV to V.

Then we applied this averaged VH$_b$R correction (called pVH$_b$R) to pEHVR and obtained pHH$_b$R, which is quite similar to the observed HH$_b$R at the target site. Basically the difference between HH$_b$R and pHH$_b$R is coming from the average operations in both EMR and pVH$_b$R calculations in five categories and so it looks obvious to have similar spectral shapes afterwards. However, our operation is solely depending on the fundamental peak frequency of microtremor HVR and theoretically speaking both EMR and pVH$_b$R should be the functions of the complex basin structure between the bedrock and the surface. By using only five categories it is quite surprising to have such a high success rate (about 80% in terms of high correlation to HHR) to have reasonable HH$_b$R prediction from a single station microtremor measurement. By introducing the proposed double correction into microtremor HVR we believe that the long-lasting doubt on the physical appropriateness and the subsequent precision issue on “Nakamura” method, that is, the direct substitute of MHVR to HH$_b$R, has been reasonably and rationally

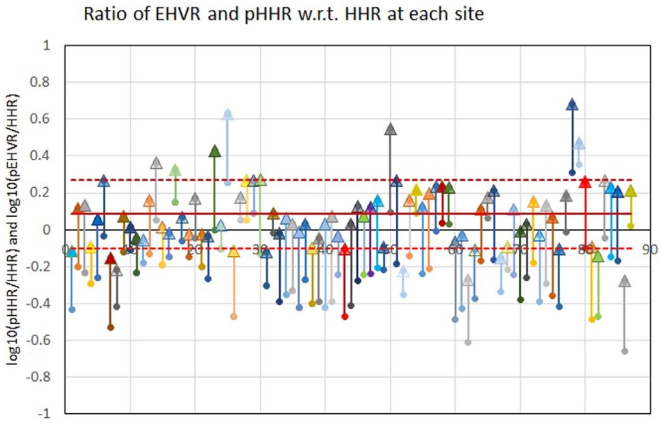

Fig. 19. Ratios of the averaged amplitudes of pHH_bR with respect to HH_bR for 100 sites, sequentially listed in the horizontal axis.

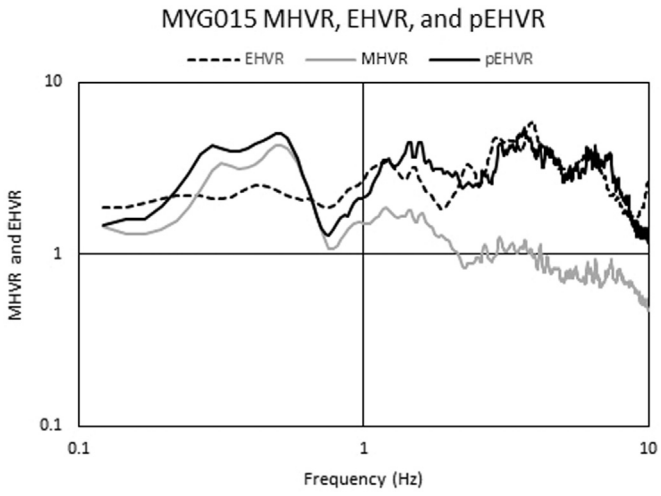

Fig. 20. Comparisons of pEHVR derived from MHVR, observed EHVR, and observed MHVR (up to 10 Hz because it was the target frequency range in [46]) at MYG015.

resolved.

In the proposed scheme we need not to perform any velocity estimates such as Vs30 translation or more rigorous velocity inversions. Once we obtain microtremor data at a target site and calculate Fourier spectra to get HVRs, then we needs only to read the fundamental peak frequency of HVR and the rest is automatic to predict a site-specific HH_bR. In application to seismically prone tectonic areas other than Japan it is desirable to obtain regional correction factors, EMR and VH_bR, based on the observed earthquake motions and microtremors in the region, since the average basin settings may be different from those of Japan. In the construction procedure of such regional correction factors we should note that we need to find a good reference site as an outcrop site of the seismological bedrock in the GIT analysis. This is very important because high-frequency amplification factors are not only controlled by the velocity structure shallower than the engineering bedrock but also by the deep basin structure down to the seismological bedrock thanks to the higher mode contributions (reverberations inside the layers). This is a strong opposition to the idea that site effects can be modeled only by the shallower structure below the site (say, down to 30 m), if our primary concern is only for the high frequency content. In our proposed method we can obtain the absolute site amplification factor for the frequency range from 0.2 to 20 Hz at the target site with respect to the seismological bedrock without having any reference information.

What is remaining to investigate is the quantitative validation exercise, including the variability (uncertainty) evaluation, using data at sites not yet used in the calculation for EMR and pVH_bR correction factors. We also need to explore the possibility to introduce regression coefficients defined as continuous functions of f_{peak} in EMR and pVH_bR correction factors once sufficient numbers of data are collected.

Acknowledgements

This study is owing to various works performed under collaboration with Shinichi Matsushima at DPRI, Kyoto University and Paco Sánchez-Sesma at IdeI, UNAM and his associates. Microtremor observations at K-NET and KiK-net stations were done by the authors with the help of students of Kawase and Matsushima laboratory in Kyushu University and Kyoto University from 2000 to 2016. A part of the study was supported by the JSPS Kakenhi Grant-in-Aid for Basic Research (A) No. 26242034. The open usage of K-NET and KiK-net earthquake data collected and distributed by NIED is highly appreciated.

Competing interests

The authors have no competing interests.

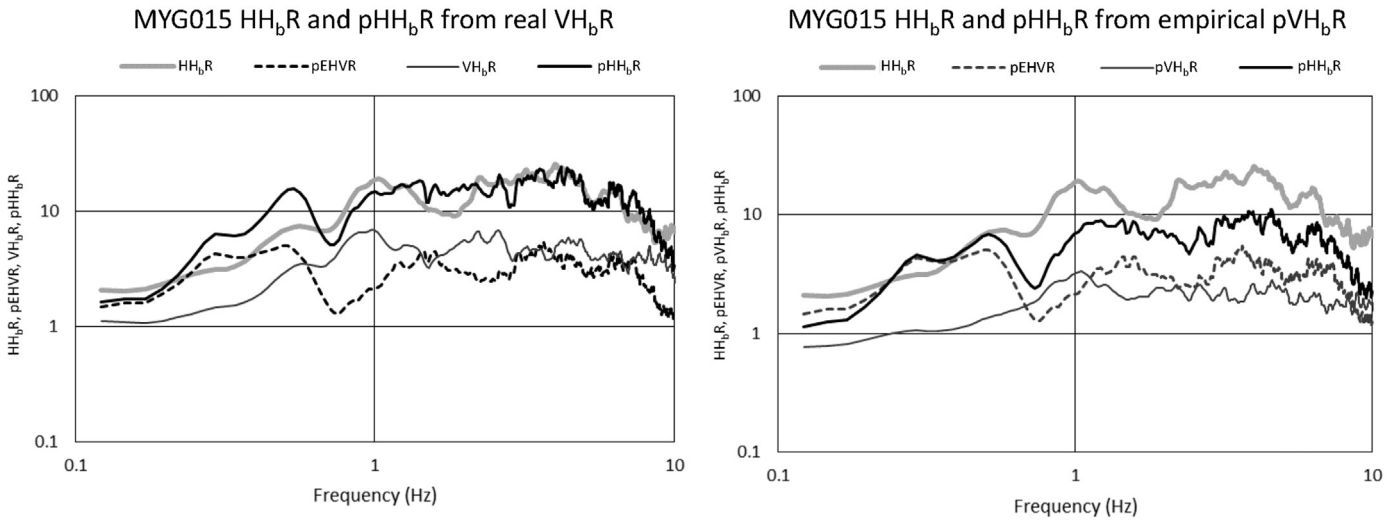

Fig. 21. Comparison of pEHVR, pHH_bR from [$pEHVR*VH_bR$], and the real HH_bR in the left-hand side panel and comparison of the same pEHVR, pHH_bR from [$pEHVR*pVH_bR$], and the same real HH_bR in the right-hand side panel.

Authors' contributions

Field investigations were performed by HK, FN, KN, and YM with the help of students in HK's laboratory in Kyushu University and Kyoto University. Microtremor analysis was performed by YM and HK. YM performed a part of the EMR analysis through discussion with HK and FN, while KN performed a port of the GIT analysis through discussion with HK and FN. All of the authors contributed to editing and revising the manuscript, and approved the final manuscript.

References

[1] Horike M. Inversion of phase velocity of long-period microtremors to the S-wave-velocity structure down to the basement in urbanized areas. J Phys Earth 1985;33:59–96.
[2] Okada H. The microtremor survey method, Geophysical Monograph Series No.12 (Volume Editor: M.W. Asten), Society of Exploration Geophysicists, Tulsa, USA.
[3] Cho I, Tada T, Shinozaki Y. Centerless circular array method: inferring phase velocities of Rayleigh Waves in broad wavelength ranges using microtremor records. J. Geophys. Res, AGU 111. 2006. p. B09315. http://dx.doi.org/10.1029/2005JB004235.
[4] Tada T, Cho I, Shinozaki Y. Beyond the SPAC method: exploiting the wealth of circular-array methods for microtremor exploration. Bull Seism Soc Am 2007;97:2080–95. http://dx.doi.org/10.1785/ 0120070058.
[5] Aki K. Space and time spectra of stationary stochastic waves, with special reference to microtremors. Bull Earthq Res Inst, Tokyo Univ 1957;35:415–56.
[6] Borcherdt RD. Estimates of site-dependent response spectra for design (methodology and justification). Earthq Spectra 1994;10:617–53.
[7] Chiou BS-J, Darragh R, Dreger D, Silva WJ. NGA project strong-motion database. Earthq Spectra 2008;24:23–44.
[8] Abrahamson NA, Silva W, Kamai R. Summary of the ASK14 ground motion relation for active crustal regions. Earth Spectra 2014;30(3):1025–55.
[9] Bozorgnia Y, Abrahamson NA, Al Atik L, Ancheta TD, Atkinson GM, Baker JW, Baltay A, Boore DM, Campbell KW, Chiou BS-J, et al. NGA-West2 research project. Earthq Spectra 2014;30:973–87.
[10] Bora SS, Scherbaum F, Kuehn N, Stafford P. On the Relationship between Fourier and response spectra: implications for the adjustment of empirical ground-motion prediction equations (GMPEs).[Published on June 2016, First Published on May 24, 2016]. Bull Seismol Soc Am 2016;106:1235–53. http://dx.doi.org/10.1785/0120150129.
[11] Steidl JH, Tumarkin AG, Archuleta RJ. What is a reference site? Bull Seism Soc Am 1996;86:1733–48.
[12] Satoh T, Kawase H, Sato T. Statistical spectral model of earthquakes in the eastern Tohoku district, Japan based on the surface and borehole records observed in Sendai. Bull Seism Soc Am 1997;87:446–62.
[13] Tucker BE, King JL. Dependence of sediment-filled valley response on input amplitude and valley properties. Bull Seismol Soc Am 1984;74(1):153–65.
[14] Andrews DJ. Objective determination of source parameters and similarity of earthquakes of different size. In: Das S, Boatwright J, Scholz CH, editors. Earthquake Source Mechanics Washington, D.C: American Geophysical Union; 1986. http://dx.doi.org/10.1029/GM037p0259.
[15] Kawase H, Matsuo H. Amplification characteristics of K-NET, KiK-net, and JMA Shindokei network sites based on the spectral inversion technique. In: Proceedings of the 13th World Conference on Earthquake Engineering, Vancouver, Canada, Paper No. 454, 1-8, 2004.8; 2004.
[16] Nakano K, Matsushima S, Kawase H. Statistical properties of strong ground motions from the generalized spectral inversion of data observed by K-NET, KiK-net, and the JMA Shindokei Network in Japan. Bul Seism Soc Am 2015;105:2662–80. http://dx.doi.org/10.1785/0120140349.
[17] Satoh T, Kawase H, Sato T. Evaluation of local site effects and their removal from borehole records observed in the Sendai region. Jpn, Bull Seism Soc Am 1995;85:1770–89.
[18] Bonilla LF, Steidl JH, Gariel J-C, Archuleta RJ. Borehole response studies at the Garner Valley Downhole array, Southern California.[Published on December 2002, First Published on December 01, 2002]. Bull Seismol Soc Am 2002;v. 92(i. 8):3165–79. http://dx.doi.org/10.1785/0120010235.
[19] Campillo M, Paul A. Long range correlations in the seismic coda. Science 2003;299:547–9.
[20] Ma S, Prieto GA, Beroza GC. Testing Community Velocity Models for Southern California Using the Ambient Seismic Field.[Published on December 2008, First Published on November 21, 2008]. Bull Seismol Soc Am 2008;98:2694–714. http://dx.doi.org/10.1785/0120080947.
[21] Shapiro NM, Campillo M. Emergence of broadband Rayleigh waves from correlations of ambient seismic noise. Geophys Res Lett 2004;31:L07614. http://dx.doi.org/10.1029/2004GL019491.
[22] Margerin L, Campillo M, Tiggelen BV, Hennino R. Energy partition of seismic coda waves in layered media: theory and application to Pinyon Flats Observatory. Geophys J Int 2009;177:571–85. http://dx.doi.org/10.1111/j.1365-246X.2008.04068.x.
[23] Kawase H, Sánchez-Sesma FJ, Matsushima S. The optimal use of horizontal-to-vertical (H/V) spectral ratios of earthquake motions for velocity structure inversions based on diffuse field theory for plane waves. Bull Seism Soc Am 2011;101:2001–14. http://dx.doi.org/10.1785/0120100263.
[24] Ducellier A, Kawase H, Matsushima S. Validation of a new velocity structure inversion method based on horizontal-to-vertical (H/V) spectral ratios of earthquake motions in the Tohoku area. Jpn, Bull Seism Soc Am 2013;103:958–70.
[25] Nagashima F, Matsushima S, Kawase H, Sánchez-Sesma FJ, Hayakawa T, Satoh T, Oshima M. Application of horizontal-to-vertical (H/V) spectral ratios of earthquake ground motions to identify subsurface structures at and around the K-NET site in Tohoku. Jpn, Bull Seism Soc Am 2014;104:2288–302. http://dx.doi.org/10.1785/0120130219.
[26] Fukihara K, Matsushima S, Kawase H. Identification of the velocity structure model of Kyoto Basin for strong motion prediction using observed earthquake and microtremor motions. J JAEE 2015;15(6):60–76. [in Japanese with English abstract].
[27] Sánchez-Sesma FJ, Rodríguez M, Iturrarán-Viveros U, Luzón F, Campillo M, Margerin L, García-Jerez A, Suarez M, Santoyo MA, Rodríguez-Castellanos A. A theory for microtremor H/V spectral ratio: application for a layered medium, Geophys. J Int Exp Lett 2011;186:221–5. http://dx.doi.org/10.1111/j.1365-246X.2011.05064.x.
[28] Lachet C, Bard P-Y. Numerical and theoretical investigations on the possibilities and limitations of Nakamura's technique. J Phys Earth 1994;42:377–97.
[29] Konno K, Ohmachi T. Ground-motion characteristics estimated from spectral ratio between horizontal and vertical components of microtremor. Bull Seismol Soc Am 1998;88:228–41.
[30] Bard P-Y. Microtremor measurements: a tool for site effect estimation? In: Proceedings of the 2nd International Symposium on the Effects of Surface Geology on Seismic Motion, Eds. Irikura, Kudo, Okada, and Sasatani, 3, Balkema, Rotterdam, 1251–1279; 1999.
[31] Bonnefoy-Claudet S, Cotton F, Bard P-Y. The nature of noise wavefield and its applications for site effects studies; A literature review. Earth-Sci Rev 2004;79:205–27.
[32] Nakamura Y. A method for dynamic characteristics estimation of subsurface using microtremor on the ground surface. Railw Tech Res Inst, Q Rep 1989;30(1):25–30.
[33] Salinas V, Luzon F, García-Jerez A, Sánchez-Sesma FJ, Kawase H, Matsushima S, Suarez M, Cuellar A, Campillo M. Using diffuse field theory to interpret the H/V spectral ratio from earthquake records in Cibeles seismic station. Mex City, Bull Seism Soc Am 2014;104:995–1001. http://dx.doi.org/10.1785/01201302.
[34] Lontsi AM, Sánchez-Sesma FJ, Molina-Villegas JC, Ohrnberger M, Krüger F. Full microtremor H/V(z,f) inversion for shallow subsurface characterization. Geophys J Int 2015;202:298–312. http://dx.doi.org/10.1093/gji/ggv132.
[35] Kawase H, Matsushima S, Satoh T, Sánchez-Sesma FJ. Applicability of theoretical Horizontal-to-Vertical ratio of microtremors based on the diffuse field concept to previously observed data. Bull Seism Soc Am 2015;105:3092–103. http://dx.doi.org/10.1785/0120150134.
[36] García-Jerez A, Piña-Flores J, Sánchez-Sesma FJ, Luzón F, Perton M. A computer code for forward calculation and inversion of the H/V spectral ratio under the diffuse field assumption. Comput Geosci 2016;97:67–78. http://dx.doi.org/10.1016/j.cageo.2016.06.016.
[37] Lermo J, Chávez-García FJ. Are Microtremors useful in site response Evaluation? Bull Seismol Soc Am 1994;84(5):1350–64.
[38] Field EH, Jacob KH. A comparison and test of various site-response estimation techniques, including three that are not reference-site dependent. Bull Seismol Soc Am 1995;85(4):1127–43.
[39] Mori Y, Matsushima S, Kawase H, Nagashima F. Comparison of observed earthquake and microtremor horizontal-to-vertical spectral ratios and inversion of velocity structures based on their empirical ratios. J Jpn Assoc Earthq Eng 2015;16(9):13–32. [in Japanese with English abstract].
[40] Lermo J, Chávez-García FJ. Site effect evaluation using spectral ratios with only one station. Bull Seismol Soc Am 1993;83(5):1574–94.
[41] Parolai S, Bindi D, Augliera P. Application of the generalized inversion technique (GIT) to a microzonation study: numerical simulations and comparison with different site-estimation techniques. Bull Seismol Soc Am 2000;90(2):286–97. [April 2000].
[42] Kinoshita S. Kyoshin Net (K-Net). Seism. Res Lett 1998;69:309–34.
[43] Aoi S, Obara K, Hori S, Kasahara K, Okada Y. New strong-motion observation network: KiK-net. Eos Trans, Am Geophys Union 2000;81:329.
[44] Okada Y, Kasahara K, Hori S, Obara K, Sekiguchi S, Fujiwara H, Yamamoto A. Recent progress of seismic observation networks in Japan -Hi-net, F-net, K-NET and KiK-net-. Earth, Planets Space 2004;56:xv–.
[45] Regnier J, Cadet H, Bonilla LF, Bertrand E, Semblat JF. Assessing nonlinear behavior of soils in seismic site response: statistical analysis on KiK-net strong motion data. Bull Seismol Soc Am 2013;103(3):1750–70.
[46] Matsushima S, Hirokawa T, De Martin F, Kawase H, Sánchez-Sesma FJ. The effect of lateral heterogeneity on horizontal-to-vertical spectral ratio of microtremors inferred from observation and synthetics. Bull Seism Soc Am 2014;104:381–93. http://dx.doi.org/10.1785/0120120321.
[47] Satoh T, Kawase H, Matsushima S. Differences between site characteristics obtained from microtremors, S-waves, P-waves and codas. Bull Seism Soc Am 2001;91:313–34.
[48] Claerbout JF. Synthesis of a layered medium from its acoustic transmission response. Geophysics 1968;33:264–9.
[49] Nakamura Y. On the H/V spectrum, 14th World Conference on Earthquake Engineering, October 2008 12-17, 2008, Beijing, China.
[50] Tuan TT, Scherbaum F, Malischewsky PG. On the relationship of peaks and troughs of the ellipticity (H/V) of Rayleigh waves and the transmission response of single layer over half-space models. Geophys J Int 2011;184:793–800.
[51] Chávez-García FJ, Manakou MV, Raptakis DG. Subsoil structure and site effects: a comparison between results from SPAC and HVSR in sites of complex geology. Soil Dyn Earthq Eng 2014;57:133–42.